ELSEVIER

Formulation and implementation of a "residual-mean" ocean circulation model

D. Ferreira *, J. Marshall

*Department of Earth Atmospheric and Planetary Sciences, Massachusetts Institute of Technology, Room 54-1515,
77 Massachusetts Avenue, Cambridge, MA 02139, USA*

Abstract

A parameterization of mesoscale eddies in coarse-resolution ocean general circulation models (GCM) is formulated and implemented using a residual-mean formalism. In that framework, mean buoyancy is advected by the residual velocity (the sum of the Eulerian and eddy-induced velocities) and modified by a residual flux which accounts for the diabatic effects of mesoscale eddies. The residual velocity is obtained by stepping forward a residual-mean momentum equation in which eddy stresses appear as forcing terms.

Study of the spatial distribution of eddy stresses, derived by using them as control parameters to "fit" the residual-mean model to observations, supports the idea that eddy stresses can be likened to a vertical down-gradient flux of momentum with a coefficient which is constant in the vertical. The residual eddy flux is set to zero in the ocean interior, where mesoscale eddies are assumed to be quasi-adiabatic, but is parameterized by a horizontal down-gradient diffusivity near the surface where eddies develop a diabatic component as they stir properties horizontally across steep isopycnals.

The residual-mean model is implemented and tested in the MIT general circulation model. It is shown that the resulting model (1) has a climatology that is superior to that obtained using the Gent and McWilliams parameterization scheme with a spatially uniform diffusivity and (2) allows one to significantly reduce the (spurious) horizontal viscosity used in coarse-resolution GCMs.
© 2005 Elsevier Ltd. All rights reserved.

Keywords: Residual-mean circulation; Eddy parameterization; Coarse-resolution ocean model

1. Introduction

In the ocean interior, mesoscale eddies are thought to be quasi-adiabatic, in the sense that eddy buoyancy fluxes tend to be directed along mean buoyancy surfaces (Gent and McWilliams, 1990; hereafter GM). The eddy transport of mean buoyancy in the ocean interior can then be represented by an eddy-induced velocity. Thus, mean buoyancy is advected by the sum of the Eulerian and eddy-induced velocities, known as the

---

* Corresponding author. Tel.: +1 617 253 7967; fax: +1 617 253 4464.
  E-mail address: dfer@ocean.mit.edu (D. Ferreira).

''residual flow''. However, close to the surface, eddy fluxes develop a diabatic component because isopycnal surfaces are maintained vertically by strong mixing while motions are constrained to be horizontal (see Marshall and Radko, 2003; Kuo et al., 2005; Ferrari and McWilliams, submitted for publication). Then, in addition to advection, mesoscale eddies can contribute a cross-isopycnal flux (a ''residual flux'') to the buoyancy equation as the surface is approached.

One can fully adopt a residual-mean framework by choosing to make the residual velocity a prognostic variable rather than the Eulerian velocity. Following Andrews and McIntyre (1976), Ferreira et al. (2005) (hereafter FMH) derive a residual-mean momentum equation for the 3-d large-scale ocean circulation. They show that, in the limit of small Rossby number, it has the same form as the primitive equations; forcing terms in the horizontal momentum equation now include an eddy contribution which has the form of a wind stress except it exists in the body of the fluid and is zero at top and bottom. This eddy stress represents the property of mesoscale eddies to redistribute momentum vertically between isopycnal layers through ''form drag'', correlations between interface displacements and pressure fluctuations. Its vertical divergence drives the eddy-induced part of the residual flow. Under certain assumptions, this forcing can be related to an eddy flux of potential vorticity (see for example Rhines and Young, 1982; Greatbatch, 1998; Wardle and Marshall, 2000). For a quasi-geostrophic zonally averaged system, the correspondence is straightforward because the eddy stress and Reynolds stress make up the components of the Eliassen–Palm flux whose divergence is the eddy potential vorticity flux (Andrews et al., 1987).

The residual-mean framework encourages us to revisit the representation of mesoscale eddies in coarse-resolution ocean climate models and provides a framework in which to improve them. We formulate and implement a simple closure for the eddy stress and residual flux. Study of the eddy stresses estimated in FMH (who used a least-squares procedure to 'solve' for the eddy stresses which brought a global ocean model into consistency with the observations) suggests that they can be represented as a down-gradient vertical momentum flux with a constant vertical viscosity. The residual eddy buoyancy flux, which is often neglected in coarse-resolution models, is parameterized as a down-gradient horizontal buoyancy flux acting over a surface diabatic layer.

A significant computational advantage of the residual-mean formulation studied here is that it is numerically more robust and requires less horizontal viscosity than traditional approaches. As pointed out by Griffies et al. (2000), the use of lateral momentum mixing in ocean models is not motivated by physical principles but only by practical contingencies, i.e. to suppress grid-point noise, maintain western boundary layers, and provide a sink of momentum at grid-scale. For example, Laplacian momentum friction – the form used in the present study – is not a realistic representation of the effects of unresolved Reynolds stresses on the resolved large-scale circulation (see, for example, the discussion in Marshall, 1981). Thus it is desirable to reduce horizontal viscosity as much as possible to maintain stability. Appealingly, the residual-mean formulation employed here allows one to significantly reduce lateral mixing of momentum.

In Section 2, we briefly derive the residual-mean equations on which our model is based. In Section 3, we describe the closures assumed for the eddy stress and the residual flux. In Section 4, numerical simulations with the residual-mean model are carried out using the MIT general circulation model (GCM) with a realistic configuration and 2.8° resolution. The model climatologies are compared with the observations and those obtained from Eulerian simulations employing the GM parameterization scheme. The effects of reduced horizontal viscosity in the residual framework are detailed in Section 5. Finally, the role of the residual flux is illustrated in Section 6. Conclusions are given in Section 7.

2. Residual-mean framework

The residual-mean theory used here is identical to that of FMH which was itself mainly inspired by Andrews and McIntyre (1976) and Treguier et al. (1997). In this section, we briefly review key elements. For more details, the reader is referred to FMH and references therein.

2.1. The residual-mean buoyancy equation

Assuming a separation between a mean (denoted by an overbar) and an eddy (denoted by a prime) fields, the mean buoyancy budget is written in the familiar form:

$$\frac{\partial \bar{b}}{\partial t} + \bar{\mathbf{v}} \cdot \nabla \bar{b} = -\nabla \cdot \overline{\mathbf{v}'b'} + \mathscr{S}, \tag{1}$$

where $\bar{\mathbf{v}}$ is the Eulerian mean velocity, $\bar{b}$ is the mean buoyancy, $\overline{\mathbf{v}'b'}$ is the eddy buoyancy flux, t is time and $\mathscr{S}$ are buoyancy sources (surface forcings and interior mixing processes). Since eddy buoyancy fluxes tend to be skew (directed parallel to $\bar{b}$ surfaces) in the ocean interior, a non-divergent eddy-induced velocity, $\mathbf{v}^\star$, can be introduced to capture their effects. The eddy-induced velocity can be written in terms of a (vector) streamfunction $\mathbf{\Psi}^\star$ thus

$$\mathbf{v}^\star = -\nabla \times \mathbf{\Psi}^\star, \tag{2}$$

where

$$\mathbf{\Psi}^\star = \left(\frac{\overline{v'b'}}{\bar{b}_z}, -\frac{\overline{u'b'}}{\bar{b}_z}, 0 \right). \tag{3}$$

Defining the residual velocities and the residual eddy flux as

$$\mathbf{v}_{\mathrm{res}} = \bar{\mathbf{v}} + \mathbf{v}^\star, \tag{4}$$

$$\mathbf{F}_{\mathrm{res}} = \overline{\mathbf{v}'b'} + \mathbf{\Psi}^\star \times \nabla \bar{b} = \frac{\overline{\mathbf{v}'b'} \cdot \nabla \bar{b}}{\bar{b}_z} \hat{\mathbf{z}}, \tag{5}$$

where $\mathbf{z}$ is a unit vector in the vertical, the mean buoyancy equation (1) becomes

$$\frac{\partial \bar{b}}{\partial t} + \mathbf{v}_{\mathrm{res}} \cdot \nabla \bar{b} = -\nabla \cdot \mathbf{F}_{\mathrm{res}} + \mathscr{S}. \tag{6}$$

Eq. (6) underscores that in a turbulent ocean it is $\mathbf{v}_{\mathrm{res}}$ and not $\bar{\mathbf{v}}$ that advects $\bar{b}$. At equilibrium, advection by the residual circulation balances the diabatic terms. Away from the surface, the diabatic sources weaken and mesoscale eddies become quasi-adiabatic ($\mathscr{S}, \mathbf{F}_{\mathrm{res}} \to 0$), and so $\mathbf{v}_{\mathrm{res}}$ tends to be along $\bar{b}$ surfaces ($\mathbf{v}_{\mathrm{res}} \cdot \nabla \bar{b} \simeq 0$, as in Kuo et al., 2005; for an example).

Complications arise near horizontal boundaries: $\mathbf{v}_{\mathrm{res}} \cdot \hat{\mathbf{n}}$ and $\mathbf{F}_{\mathrm{res}} \cdot \hat{\mathbf{n}}$ (where $\hat{\mathbf{n}}$ is a unit normal to the boundary) are not necessarily zero even though $\overline{\mathbf{v}'b'} \cdot \hat{\mathbf{n}} = 0$. Following Treguier et al. (1997) and Ferrari and McWilliams (submitted for publication), we can make progress by considering a surface layer of thickness h_s in which eddy buoyancy fluxes veer from along-isopycnal to horizontal as the sea surface is approached (see Fig. 1). In this layer, eddy fluxes develop a strong diabatic component since isopycnal surfaces are maintained steep by small scale turbulent mixing. This diabatic surface layer encompasses the mixed layer, but also includes a transition layer connecting the base of the mixed layer to the low-mixing region of the ocean interior below (see Section 3.2 for a further discussion).
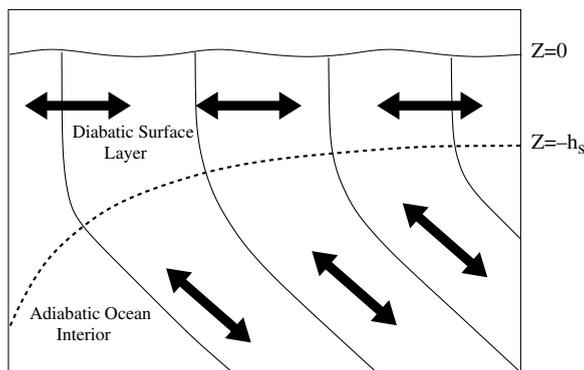

Fig. 1. Schematic representation of the relationship between isopycnal surfaces (solid) and eddy buoyancy fluxes (arrows) in the ocean. Note that the diabatic surface layer may extend deeper than the mixed layer.

Assuming that the eddy-induced flow of the interior is returned within the diabatic layer, the definition of $\Psi^{\star}$ is modified to

$$\Psi^{\star} = \left(\frac{\overline{v'b'}}{\bar{b}_z}, -\frac{\overline{u'b'}}{\bar{b}_z}, 0 \right) \Bigg|_{z=-h_s} \mu, \quad -h_s < z < 0, \tag{7}$$

where μ is a function that changes from 0 at the surface to 1 at $z = -h_s$. Note that μ and h_s can be functions of space and time.

The residual flux $\mathbf{F}_{res}$ is obtained directly from the first part of Eq. (5). A similar diabatic layer can be defined at the bottom of the ocean. Note that $\mathbf{v}_{res}$ and $\mathbf{F}_{res}$ remain unchanged in the interior, but they satisfy a no-normal flux condition at top and bottom, i.e. $\Psi^{\star} = \mathbf{0}$ at all boundaries.

2.2. The residual momentum equation

Along with the residual-mean buoyancy equation, we must formulate the residual-mean momentum equation. It is useful to first consider the momentum equation in the planetary geostrophic limit, in which advection of momentum is neglected entirely

$$f\hat{\mathbf{z}} \times \bar{\mathbf{v}} = -\frac{1}{\rho_0} \nabla p + \frac{1}{\rho_0} \frac{\partial \boldsymbol{\tau}^{w}}{\partial z}, \tag{8}$$

where f is the Coriolis parameter, p is the pressure, ρ_0 is a constant reference density and $\boldsymbol{\tau}^{w}$ is the surface wind stress. Since from Eq. (4), $\bar{\mathbf{v}} = \mathbf{v}_{res} + \nabla \times \Psi^{\star}$, the above may be written

$$f\hat{\mathbf{z}} \times \mathbf{v}_{res} = -\frac{1}{\rho_0} \nabla p + \frac{1}{\rho_0} \frac{\partial (\boldsymbol{\tau}^{w} + \boldsymbol{\tau}^{e})}{\partial z}, \tag{9}$$

where, using Eq. (2), we identify

$$\boldsymbol{\tau}^{e} = (\tau_x^{e}, \tau_y^{e}) = \rho_0 f \Psi^{\star} \tag{10}$$

as an eddy stress which vanishes ($\Psi^{\star} = \mathbf{0}$) at the top and bottom of the ocean (see Section 2.3 for a physical interpretation).

If the advection of momentum is not neglected, we may write the time-mean momentum budget thus

$$\frac{\partial \bar{\mathbf{v}}}{\partial t} + \bar{\mathbf{v}} \cdot \nabla \bar{\mathbf{v}} + f\hat{\mathbf{z}} \times \bar{\mathbf{v}} = -\frac{1}{\rho_0} \nabla p + \frac{1}{\rho_0} \frac{\partial \boldsymbol{\tau}^{w}}{\partial z} - \overline{\mathbf{v}' \cdot \nabla \mathbf{v}'}, \tag{11}$$

where the last term on the rhs are Reynold stresses due to eddies. Since the residual velocity has the same magnitude as the Eulerian velocity[1] and the advection terms in Eq. (11) are already order Rossby number (R_0) relative to the Coriolis terms, we may replace $\bar{\mathbf{v}}$ in the advection terms by $\mathbf{v}_{res}$. Thus, to leading order in R_0, the momentum equation becomes

$$\frac{\partial \mathbf{v}_{res}}{\partial t} + \mathbf{v}_{res} \cdot \nabla \mathbf{v}_{res} + f\hat{\mathbf{z}} \times \mathbf{v}_{res} \simeq -\frac{1}{\rho_0} \nabla p + \frac{1}{\rho_0} \frac{\partial (\boldsymbol{\tau}^{w} + \boldsymbol{\tau}^{e})}{\partial z} - \overline{\mathbf{v}' \cdot \nabla \mathbf{v}'}, \tag{12}$$

where $\boldsymbol{\tau}^{e}$ is given by Eq. (10). Eq. (12) retains the primitive equation form because we have kept some, but not all of the O(R_o) terms. This is not an issue as long as the O(R_o) terms are negligible, as is typical in coarse resolution models such as the one used here (see description in Section 3.1). Note that we do not assume quasi-geostrophic scaling. However, it is also important to note that Eq. (12) does not hold in general and must only be used in appropriate circumstances. Finally, Reynolds stress terms are replaced by a viscosity v acting on the horizontal flow. This is typically assumed in large-scale ocean models, has no physical justification, but is required for numerical stability.

---

[1] To see this, suppose that $b' \sim \bar{b}_z \eta'$ where η' is the isopycnal displacement, we find that $\frac{\partial}{\partial z}\left(\frac{\overline{v'b'}}{\bar{b}_z}\right) \sim \frac{r\eta'\bar{v}}{H}$ where r is the ratio of the eddy to the mean velocity $\frac{v'}{\bar{v}}$ and H, the vertical scale of mesoscale eddies. Thus $\mathbf{v}_{res} = \bar{\mathbf{v}}(1 + O(\frac{r\eta'}{H}))$. Taking $H \sim 1000$ m and $\eta' \sim 100$ m, $\frac{r\eta'}{H}$ remains less than unity since r ranges typically from 1 in jets to 10 in the interior of gyres.

In summary, then, we adopt the following residual momentum balance appropriate to the large scale:

$$\frac{\partial \mathbf{v}_{\text{res}}}{\partial t} + \mathbf{v}_{\text{res}} \cdot \nabla \mathbf{v}_{\text{res}} + f\hat{\mathbf{z}} \times \mathbf{v}_{\text{res}} = -\frac{1}{\rho_0}\nabla p + \frac{1}{\rho_0}\frac{\partial(\boldsymbol{\tau}^{\text{w}} + \boldsymbol{\tau}^{\text{e}})}{\partial z} + v\nabla^2 \mathbf{v}_{\text{res}}. \tag{13}$$

Eq. (13) has the same form as the 'primitive equation', albeit with a reinterpretation of the terms (residual, rather than Eulerian mean velocities). The forcing term on the rhs has an eddy contribution which has exactly the same status as the wind stress, except that it exists in the interior of the fluid and vanishes at the upper and lower boundaries.

We call the key equations of our model – (6), (10) and (13) – the 'Transformed Eulerian Mean' (TEM) or residual-mean equations. They are the form used in FMH.

2.3. Physical interpretation of eddy stresses

In the zonal average theory, the eddy stress (3) has clear connections to:

(1) the vertical component of the Eliassen–Palm flux (see Andrews et al., 1987),
(2) the stretching component of an eddy potential vorticity flux (e.g., Marshall, 1981),
(3) the eddy form stress resulting from the correlation between eddy pressure fluctuations p' and isopycnal displacements η': $\rho_0 f\frac{\overline{v'b'}}{\bar{b}_z} \sim \rho_0 f\overline{v'\eta'} \sim \overline{p'_x\eta'}$ using geostrophic balance (see Rhines, 1979). For example, a positive zonal eddy stress corresponds to a downward flux of eastward momentum.

3. Eddy closure

To close the TEM system, we must parameterize the eddy stress in the ocean interior, the depth of the surface diabatic layer h_{s}, the tapering μ within that layer and the residual flux. We must also describe the eddy parameterization employed for tracers other than buoyancy.

Before going further, we make some simplifying assumptions. As discussed in the introduction, we first assume that the residual flux is negligible in the ocean interior: that is, eddy fluxes are well approximated by their adiabatic component. Secondly, we assume that eddy fluxes are vanishingly small in the deep ocean and set the eddy stress to zero at the bottom without the use of tapering. This is equivalent to assuming that the bottom diabatic layer is embedded in the lowest model layer. For the same reason, the residual flux at the bottom is neglected.

3.1. Eddy stress as a vertical mixing of momentum

We assume that eddy buoyancy fluxes are directed down the mean buoyancy gradient. Although, in general, the diffusivity relating the eddy fluxes to the mean gradient has the form of a tensor, we follow GM here and choose a (simple) scalar diffusivity κ:

$$\overline{\mathbf{v}'b'} = -\kappa\nabla_h\bar{b}. \tag{14}$$

Using the thermal wind relationship, the eddy stress (10) can be expressed in terms of the vertical shear of the current, thus

$$(\tau_x^{\text{e}}, \tau_y^{\text{e}}) = \rho_0 f^2 \frac{\kappa}{N^2}(u_z, v_z) \tag{15}$$

and so

$$\frac{1}{\rho_0}\frac{\partial(\tau_x^{\text{e}}, \tau_y^{\text{e}})}{\partial z} = \frac{\partial}{\partial z}\left(v_{\text{e}}\frac{\partial}{\partial z}\right)(u, v) \tag{16}$$

with

$$v_e = \kappa \frac{f^2}{N^2} = \alpha f^2 \tag{17}$$

is a vertical mixing of momentum. Note that in Eq. (17) we have taken out the known dependence of f^2 and isolated the remaining, less certain dependencies, into a parameter α.

Greatbatch and Lamb (1990) made an heuristic derivation of Eq. (15) based on the correspondence in quasi-geostrophic theory between vertical mixing of momentum and horizontal mixing of potential vorticity (Rhines and Young, 1982). They did not make the link with residual-mean theory, although this was later revisited by Greatbatch (1998). Gent et al. (1995) showed that the GM parameterization scheme, when cast in terms of the 'effective transport velocity' – the residual flow – is equivalent to an eddy stress of the form (15) in the planetary quasi-geostrophic limit.

Here we will further assume that it is the residual momentum that is mixed rather than the momentum evaluated geostrophically: we modify Eq. (16) thus

$$\frac{1}{\rho_0} \frac{\partial(\tau_x^e, \tau_y^e)}{\partial z} = \frac{\partial}{\partial z} \left(v_e \frac{\partial}{\partial z} \right) (u_{res}, v_{res}). \tag{18}$$

We now test relation (18) directly using the results of FMH. Employing a residual-mean ocean model formulated as in Section 2 (except for the neglect of $\mathbf{F}_{res}$) and using a least-squares procedure, FMH estimated the 3D eddy stresses which minimizes the departure of the model temperature from climatological temperature observations. Fig. 2 shows the averaged vertical profiles of the quantities $\tau_x^e/(\rho_0 f^2)$ and $\alpha \partial u_{res}/\partial z$ from the optimized solution of FMH with $\alpha = 2 \times 10^8$ m^2 s. Only locations where the inferred κ is positive are included – the Southern Ocean (south of 30° S) and the Northern western boundary currents (30°–45° N). The two quantities are very close to each other from a depth of about 150 m down to the sea floor. Fitting the two curves for near surface points would require a much smaller α. This can be interpreted as an indication of a "built-in" tapering of the optimized eddy stress or of the presence of a diabatic layer near the surface. These near-surface points can be discarded as the eddy stress closure (17) is only sought for the ocean interior. In the diabatic surface layer, the eddy stress is determined by the tapering scheme equation (7).

For α constant, the eddy viscosity v_e is thus independent of depth and longitude, varying only with latitude. Note that, because of the thermal wind relationship employed to derive Eq. (17) and the small Rossby number
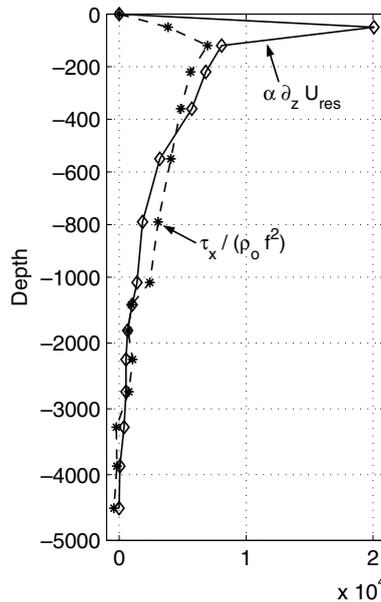

Fig. 2. Averaged vertical profile of $\tau_x/(\rho_0 f^2)$ (dashed) and $\alpha \partial_z u_{res}$ (solid) with α set to 2×10^8 m^2 s from the optimized solution of FMH. The averaging area extends south of 30° S and from 30° N to 45° N where the inferred eddy diffusivities are mainly positive.

approximation used to derive Eq. (12), v_e, and hence the eddy stress and eddy-induced streamfunction, vanish at the equator. This is unlikely to happen in the real ocean because mesoscale activity (such as tropical instability waves) is a feature of tropical dynamics. Nevertheless, we do not attempt to modify our parameterization at the equator and allow the eddy stress to vanish there. We note in passing that it may be desirable and perhaps necessary to modify our residual-mean formulation for treatment of equatorial dynamics.

As noted above, the parameterizations (16) and then (18) – provided the geostrophic shear is well approximated by the residual shear – are equivalent to the GM parameterization in the planetary quasi-geostrophic limit. An equivalent thickness diffusivity κ_{gm}^{eq} to these parameterizations is given by (17):

$$\kappa_{gm}^{eq} = \alpha N^2. \tag{19}$$

(Note this is only valid outside the diabatic layer.) If α is independent of depth, Eq. (19) suggests that the eddy diffusivity varies as N^2. Indeed, FMH observed that the estimated eddy diffusivity is surface intensified and has a vertical profile similar to that of the stratification N^2 (see their Fig. 13). As noted by FMH, the surface intensification of the eddy diffusivity is perhaps best rationalized by a steering level argument (Green, 1970). The latter argues that κ should peak at the steering level of unstable modes where the phase speed of eddies equals the mean flow velocity and eddy-mean interaction is maximized. Gill et al. (1974) conducted a linear stability analysis of various exponential profiles of stratification and velocity. They found that, in the case of baroclinic instability, the steering level was very close to the surface (within the top 500 m) as was the region of maximum extraction of mean potential energy. An N^2-dependence of the eddy diffusivity is more difficult to rationalize. FMH noted that such a dependence results in an eddy stress collocated in space with the surface winds and currents rather than the isopycnal slopes. This was critical to the dynamical balance of, for example, the Antarctic circumpolar current (ACC) because the eddy stress then transports the surface input of momentum by the wind downward where it can be balanced by pressure gradients across topographic features. However, linear stability analysis suggests that surface intensified eddy amplitudes results from the surface intensification of the current shear rather than the stratification (Gill et al., 1974; Vallis, 2005, personal communication). The key point, however, is perhaps not the precise dependence of κ on N^2 and/or the flow, but that it is surface intensified.

3.2. Diabatic surface layer

The diabatic surface layer encompasses the mixed layer and Ekman layer, but should also include a transition layer connecting the base of the mixed layer to the low-mixing region of the ocean interior (Treguier et al., 1997; Ferrari and McWilliams, submitted for publication). We lack observations as well as a theoretical framework to describe the diabatic surface layer.

The transition layer can be identified as the region where isopycnal surfaces can be lifted into the mixed layer under the heaving of mesoscale eddies and thus exposed to strong diabatic processes. The isopycnal displacement η' is given approximately by

$$\eta' = \frac{b'}{\bar{b}_z}. \tag{20}$$

Assuming that buoyancy anomalies scale as a mixing length L_e (taken to be the first Rossby radius of deformation) times the mean horizontal buoyancy gradient, the isopycnal displacement is given by $S_\rho L_e$ where S_ρ is the isopycnal slope. For $S_\rho = 10^{-3}$–10^{-2} and $L_e = 25$ km, this scaling suggests that the transition layer extends typically 25–250 m below the mixed layer. Note that the depth of the diabatic layer is expected to vary in time and space. However, it is unlikely that near-surface eddy fluxes should be sensitive to synoptic mixed-layer depth fluctuations, but rather a time average of them. Readers are referred to Ferrari and McWilliams (submitted for publication) for a more extensive discussion of the diabatic surface layer.

At this stage, approximating the diabatic layer by the mixed layer is probably the most appropriate, and certainly the most pragmatic, choice. However, because of the coarse vertical resolution of our model (see below), the diagnostic of the mixed-layer depth is rather crude. Therefore, in the present study, we simply set $h_s = 120$ m, which corresponds to the top two layers of our model.

3.3. The tapering function μ

We also make a simple choice of the tapering function μ: it is assumed to be linear, varying from 0 at the surface to 1 at $h_s = 120$ m. The eddy-induced velocity then has no vertical shear in the diabatic layer and does not contribute to restratify the mixed layer (as long as the latter is shallower than 120 m).

Our choice of μ is similar to that of Treguier et al. (1997). Ferrari and McWilliams (submitted for publication) also prefer to have no shear in the eddy-induced velocity in the mixed layer and a linear profile in the transition layer (parabolic profile for the eddy-induced streamfunction). Although more detailed, this choice demands that one distinguishes between the mixed layer and the transition layer. Once again, in view of the coarse vertical resolution of our model, our simple choice is preferred here.

3.4. The residual flux F_{res}

Near the surface, eddies stir tracer properties along the boundary and across nearly vertical isopycnal (see Marshall and Radko, 2003; Radko and Marshall, 2003; Kuo et al., 2005). Here, we represent the residual flux in the diabatic surface layer by a horizontal down-gradient flux with a diffusivity coefficient κ_s. As noted above, the residual flux is set to zero in the ocean interior. The residual-mean buoyancy equation (6) then becomes

$$\frac{\partial \bar{b}}{\partial t} + \mathbf{v}_{\text{res}} \cdot \nabla \bar{b} = \mathscr{S} + \nabla_h \cdot [\kappa_s \nabla_h \bar{b}], \tag{21}$$

1where κ_s is zero in the ocean interior.

3.5. Tracer equation

Practical implementation of our parameterization schemes requires an equation for temperature and salinity (because buoyancy is not a prognostic variable) and for passive tracers.

Plumb (1979) showed that, in the limit of small amplitudes eddies, the eddy-induced velocity is in fact the same for all tracers. Accordingly, here it is assumed that all tracers are advected by the same residual velocity given by Eq. (13). In addition, tracers are stirred along isopycnal surfaces by mesoscale eddies. This is represented by an isopycnal mixing tensor $\mathscr{R}$ (Redi, 1982). Thus, the equation for a general tracer c is:

$$\frac{\partial \bar{c}}{\partial t} + \mathbf{v}_{\text{res}} \cdot \nabla \bar{c} = \mathscr{S}_c + \mathscr{R}(\bar{c}), \tag{22}$$

where $\mathscr{S}_c$ is the source and sink of the tracer. The residual flux is implemented by rotating back the isopycnal tensor $\mathscr{R}$ to the horizontal for temperature and salinity in the surface diabatic layer. This results in a horizontal mixing of buoyancy just at the surface since $\mathscr{R}(\bar{b}) = 0$ by definition.

4. Experiments with a coarse-resolution ocean model

4.1. The MITgcm

To test the proposed parameterization, we carry out a series of experiments using the MITgcm (Marshall et al., 1997a,b). The model has a horizontal resolution of 2.8° and 15 levels in the vertical. The geometry is 'realistic' except for the absence of the Arctic Ocean; bathymetry is represented by partial cells (Adcroft et al., 1997). The model is forced by observed monthly mean climatological surface wind stresses from Trenberth et al. (1990), and observed monthly mean climatological heat fluxes and annual-mean evaporation–precipitation (Jiang et al. (1999)). Sea surface temperature and salinity are restored toward observed monthly mean climatological values (Levitus and Boyer, 1994; Levitus et al., 1994) with time scales of 2 and 3 months, respectively. However, no representation of sea-ice is included. Convection is parameterized by enhanced vertical diffusion whenever the water column becomes statically unstable. The vertical diffusion and viscosity are
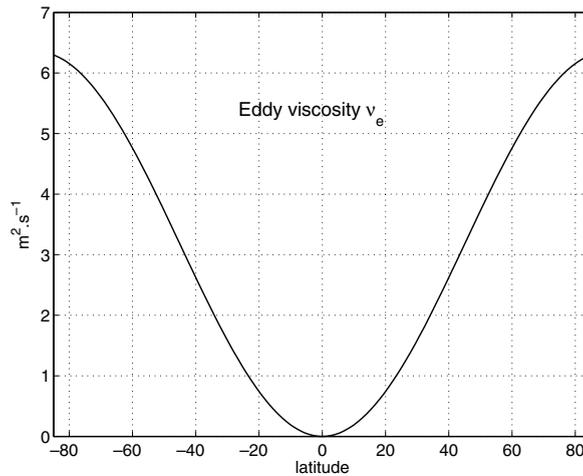
Fig. 3. Meridional profile of the eddy viscosity v_e (in $m^2 s^{-1}$) for $\alpha = 3 \times 10^8 \ m^2$ s.

set at $5 \times 10^{-5} \ m^2 \ s^{-1}$ and $10^{-3} \ m^2 \ s^{-1}$, respectively. The latter is negligible compared to the eddy vertical viscosity v_e, but is retained for comparison with our Eulerian mean runs. The isopycnal diffusion κ_I used in $\mathscr{R}$ is set to $1000 \ m^2 \ s^{-1}$. Tapering of isopycnal slopes is done adiabatically using the scheme of Gerdes et al. (1991).

In the residual model, α is set to $3 \times 10^8 \ m^2$ s with the resulting meridional profile of v_e shown in Fig. 3: v_e increases from 0 at the equator to about $6 \ m^2 \ s^{-1}$ at the poles. As noted above, the depth of the diabatic layer is uniformly set to 120 m and the function μ is assumed to be linear within it. Details of the numerical implementation of the eddy stress are given in Appendix A.

For comparison, the model is also run in a standard 'Eulerian' configuration. In this case, the adiabatic effects of mesoscale eddies are represented by the eddy-induced transport of GM (the tapering is again carried out with the Gerdes et al. (1991) scheme). Two different thickness diffusion coefficients κ_{gm} are used: a uniform coefficient κ_{gm}^u set to $1000 \ m^2 \ s^{-1}$ and a N^2-dependent coefficient $\kappa_{gm}^{N^2}$. Following the implementation of FMH, the latter is given by

$$\kappa_{gm}^{N^2} = \frac{N^2}{N_{ref}^2} \kappa_{ref}, \qquad (23)$$

where N_{ref}^2 is the reference stratification at the interface of the first and second model levels, and $\kappa_{ref} = 4000 \ m^2 \ s^{-1}$. To avoid singularities – for example when N_{ref}^2 goes to zero during a convective event – the ratio N^2/N_{ref}^2 is tapered to 1.

To make unbiased comparison between the residual model and the Eulerian runs (called *Res*, *GM* and *GM_N2*), each configuration was tuned using its eddy parameterization to obtain the best possible climatology. These three configurations are first run with a horizontal viscosity of $5 \times 10^5 \ m^2 \ s^{-1}$. This reference value is required in the Eulerian form to obtain an acceptable numerical solution (see Section 5). We also carry out two complementary experiments, *ReslAh* and *GMlAh*, with a low horizontal viscosity, reduced by one order of magnitude to $5 \times 10^4 \ m^2 \ s^{-1}$.

To simplify the comparison between the residual and Eulerian runs, all the above experiments are realized without a residual flux in the diabatic layer. To test the latter, it is included in a TEM calculation with low viscosity *ReslAhF*. This is done by replacing the isopycnal diffusion with a horizontal one in the diabatic surface layer. The horizontal diffusivity κ_s is set to $1500 \ m^2 \ s^{-1}$ there. Estimates of the surface horizontal diffusivity in the Southern Ocean by Marshall et al. (in press) have strong spatial dependence with values ranging from 500 to $2000 \ m^2 \ s^{-1}$. Our choice is somewhat on the higher end of this range.

All simulations are initialized with the Levitus climatology and run for 7000 years until they are close to equilibrium. A summary of all experiments is given in Table 1.

Table 1
Summary of the experiments: for each run, we indicate the eddy parameterization, horizontal viscosity and residual flux, temperature (J_T) and salinity (J_S) cost functions, and transport at Drake Passage (TDP in Sv)

	Eddy	A_h	F_{res}	J_T	J_S	TDP
GM	GM Bolus velocity uniform κ	5×10^5	No	153	166	106
GM_KN2	GM Bolus velocity N^2-dependent κ	5×10^5	No	85	55	110
GMlAh	Bolus velocity uniform κ	5×10^4	No	171	222	111
Res	Residual form with eddy stress	5×10^5	No	85	86	111
ReslAh	Residual form with eddy stress	5×10^4	No	72	76	124
ReslAhF	Residual form with eddy stress	5×10^4	Yes	112	133	126

4.2. Temperature and salinity

To compare the climatology of the various runs, we introduce a cost function. Such functions, often used in optimization problems (Stammer et al., 2002; FMH), provide a straightforward and objective way to evaluate the quality of the model. For example, the temperature cost function J_T measures the departure of the model temperature from climatological observations (Levitus and Boyer, 1994):

$$J_T = \frac{1}{N} \sum_{i=1}^{N} \left[\frac{\overline{T}_i - \overline{T}_i^{\text{lev}}}{\sigma_i^T} \right]^2, \tag{24}$$

where $\overline{T}_i$ is the mean model temperature at equilibrium and $\overline{T}_i^{\text{lev}}$, the annual mean observed temperature at each grid point i. The differences are weighted by an a priori uncertainty σ_i^T of observations (as given by Levitus and Boyer, 1994). The error σ_i^T is only a function of depth and varies from 0.5 K at the surface to 0.05 K at the bottom, mainly reflecting the decreasing temperature variance with depth. A value of J_T of order 1 means that the model is, on average, within observational uncertainties. Similarly, a salinity cost function J_S can be defined with the salinity uncertainty also decreasing downward from 0.14 psu at the surface to 0.01 psu below a depth of 3500 m. Values of the temperature and salinity cost functions are summarized in Table 1.

The annual mean temperature and salinity fields are significantly closer to observations in the *Res* run than in *GM*, the cost functions being smaller by roughly a factor of 2. Figs. 4 and 5 show the zonal mean departure of the model temperature and salinity from observations for experiments *Res* and *GM*. The warm bias of thermocline water and the cold bias of deep water seen in *GM* are reduced by a factor of 2 in *Res*. Deep water masses of the *GM* run are too fresh, while Antarctica Intermediate Water is too salty (a common bias seen in coarse-resolution GCMs). Both errors are reduced in the residual-mean formulation *Res*. However, the properties of surface water (down to about 200 m) are unchanged, likely due to the use of restoring boundary conditions. It should also be noted that the *Res* solution is slightly degraded in some places compared to that of *GM* (e.g. the temperature at 50° N at 300 m or salinity around Antarctica).

The salinity field of the Eulerian experiment with a N^2-dependent diffusivity *GM_N2* is slightly better than the *Res* one while their temperature fields are very similar (see Figs. 4 and 5, and Table 1). As mentioned in Section 3.2, the eddy closure (18) used in the residual model *Res* is equivalent, within some approximations, to an Eulerian formulation with a N^2-dependent diffusivity (see (19)). The similarity of *Res* and *GM_N2* would then suggest that their improvement relative to the *GM* run results mainly from the surface-intensified (implicit or explicit) eddy diffusivity they adopt.

4.3. Eddy diffusivity

To verify this, we diagnose the eddy diffusivities of the *Res* and *GM_N2* runs. In *Res*, the equivalent eddy diffusivity κ_{gm}^{eq} is not computed from its theoretical value (19). Rather, it is estimated directly by dividing the meridional eddy-induced streamfunction by the meridional slope. In *GM_N2*, the eddy diffusivity $\kappa_{gm}^{N^2}$ is a variable of the model. Zonal means of κ_{gm}^{eq} and $\kappa_{gm}^{N^2}$ are shown in Figs. 6 and 7, respectively.
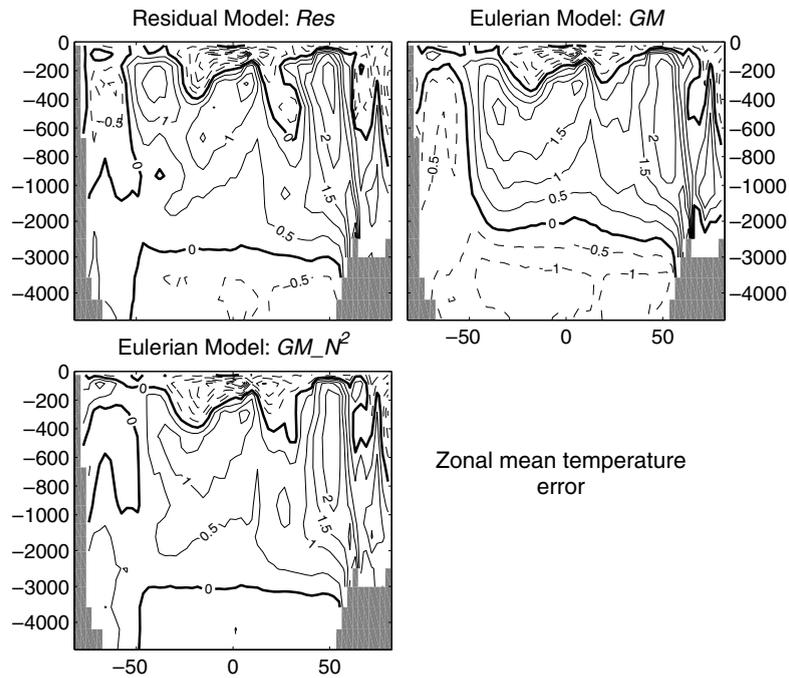
Fig. 4. Zonal mean departure of temperature from climatological observations (Levitus dataset) for the residual-mean run *Res* (top left), the Eulerian run with uniform eddy diffusivity *GM* (top right), and the Eulerian run with a N^2-dependent eddy diffusivity *GM_N2* (bottom).
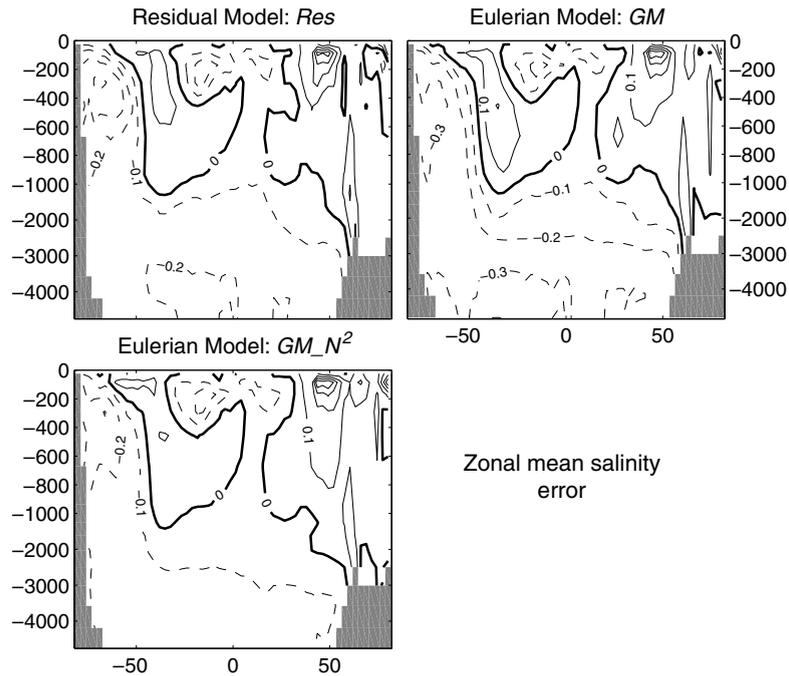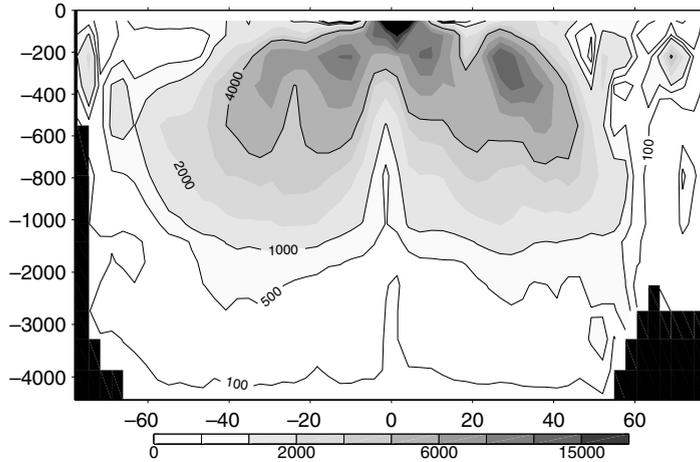

Fig. 5. Same as Fig. 4 but for salinity.

Fig. 6. Zonal mean equivalent eddy diffusivity κ_{gm}^{eq} (in m^2 s^{-1}) of the *Res* run. It is estimated by dividing the meridional eddy-induced streamfunction by the meridional slope.
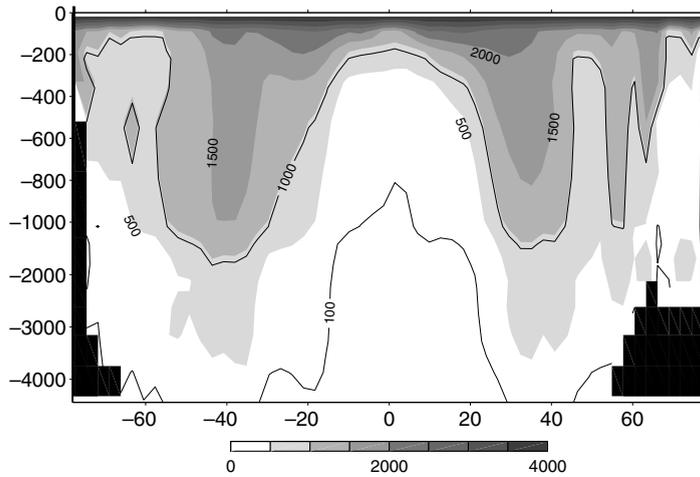

Fig. 7. Zonal mean horizontal eddy diffusivity (in m^2 s^{-1}) of the *GM_N2* run employing a N^2-dependent eddy diffusivity (Eq. (23)) in the GM parameterization scheme.

The equivalent diffusivity κ_{gm}^{eq} of the *Res* run is small at depth (about 100 m^2 s^{-1}) and increases upward to reach a maximum in subsurface (between 0 and 500 m depending of the latitude). This maximum ranges from 1000 to up to 15,000 m^2 s^{-1} in the tropics. The estimated value of κ_{gm}^{eq} is very close to its theoretical value (19) everywhere expect near the surface. Indeed, Eq. (19) suggests that κ_{gm}^{eq} should peak at the surface, similarly to $\kappa_{gm}^{N^2}$. This discrepancy arises for two reasons: (1) the presence of the tapering function μ in which Eq. (19) does not hold and (2) the approximation of the geostrophic shear by the residual shear in Eq. (18). Near the surface, the residual shear can be significantly smaller than the geostrophic one (albeit of the same sign), leading to smaller eddy diffusivities than predicted by (19). The diffusivity $\kappa_{gm}^{N^2}$ is also small near the bottom (100 m^2 s^{-1} or less) and increases to 4000 m^2 s^{-1} at the surface. Because the stratification in the tropics is very surface-intensified, the diffusivity decreases sharply and is smaller than 500 m^2 s^{-1} below 400 m depth. In contrast, the diffusivity in the midlatitude diminishes more gently and is still about 500 m^2 s^{-1} at 3500 m. At high latitudes, the near-surface stratification is relatively large compared to deeper values because of the salinity minimum. As in the tropics, this results in small diffusivity below 400 m.

The major differences between $\kappa_{gm}^{N^2}$ and κ_{gm}^{eq} result from the choice of Eq. (23) to implement the N^2-dependence in *GM_N2*. By construction, $\kappa_{gm}^{N^2}$ is identically equal to κ_{ref} at the surface and decreases downward. On the other hand, κ_{gm}^{eq} varies at the surface as shown by the approximation Eq. (19). As a consequence, κ_{gm}^{eq} is much larger than $\kappa_{gm}^{N^2}$ in the tropics while outside the tropics, the two diffusivities are rather similar.

More importantly, both diffusivities are surface intensified, with values substantially higher (near the surface) and lower (at depth) than the (uniform) 1000 $m^2\,s^{-1}$ commonly used in coarse-resolution model (and in our *GM* experiment). These spatial variations significantly modifies the eddy-induced circulation compared to the case of uniform diffusivity.

4.4. Meridional overturning circulation

The Eulerian, eddy-induced and residual overturning streamfunctions for *Res*, *GM*, and *GM_N2* are shown in Figs. 8–10 respectively. In *GM* and *GM_N2*, the Eulerian and eddy-induced circulations are explicitly resolved and the residual is computed as their sum. In the residual-mean run *Res*, the residual circulation is the prognostic variable and the eddy-induced circulation is obtained as the zonal integral of $\tau_x^e/(f\rho_0)$. The Eulerian circulation is then diagnosed from their difference.
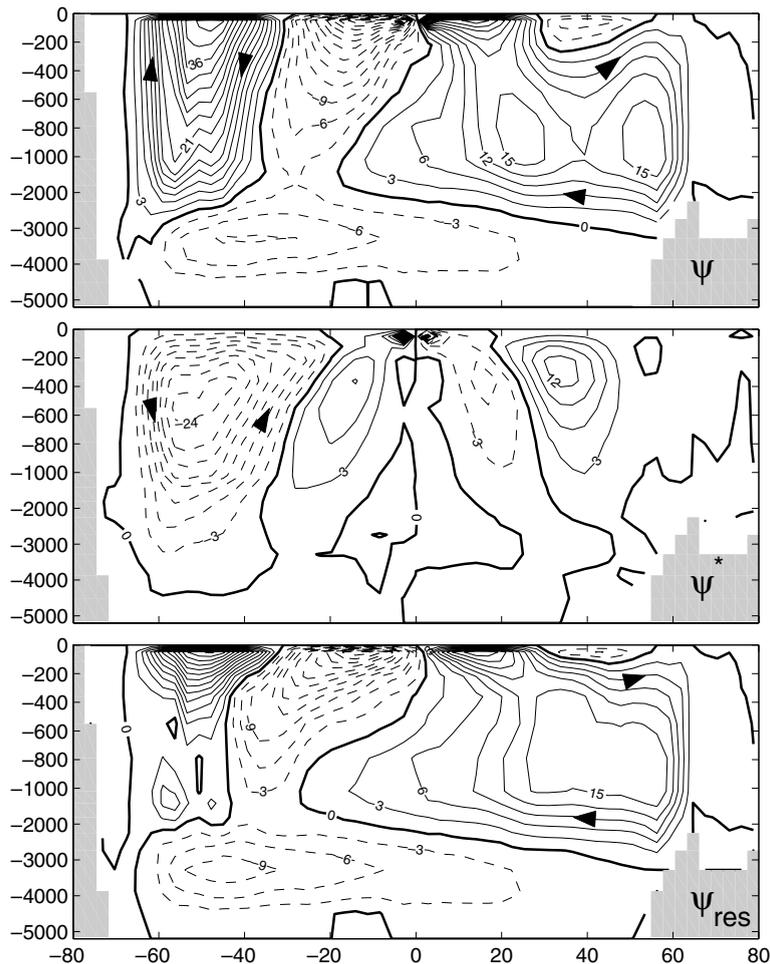

Fig. 8. Eulerian (top), eddy-induced (middle) and residual (bottom) meridional overturning circulation for the residual run *Res*. Details are given in the text. The contour interval is 3 Sv. Solid and dashed lines are positive and negative values, respectively. The zero contour is thick black.
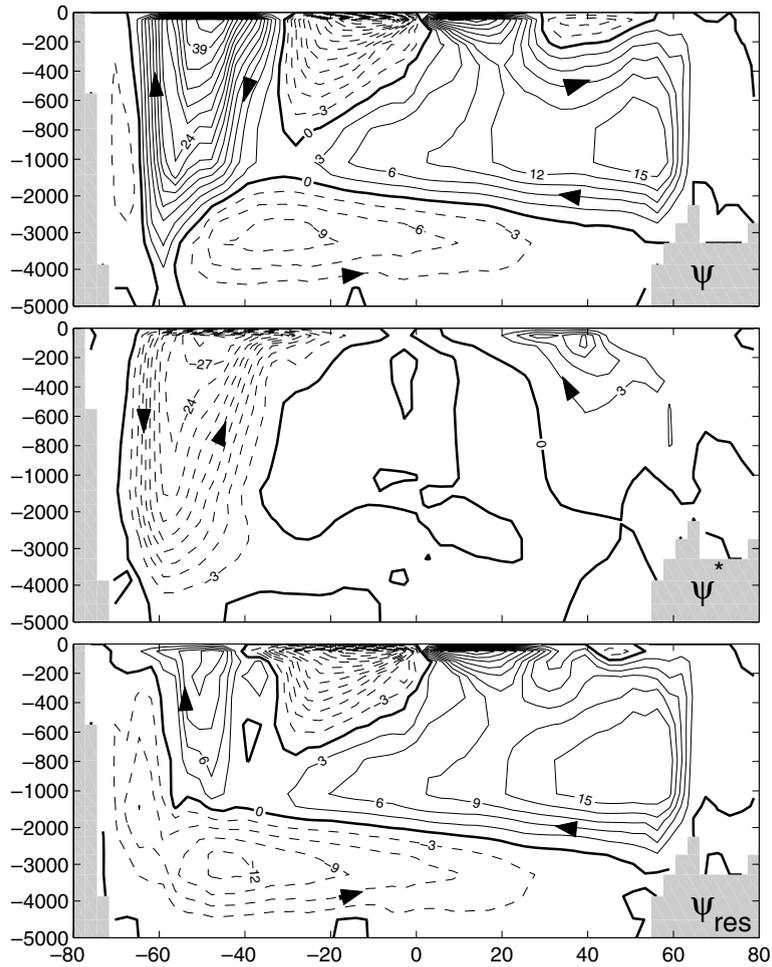
Fig. 9. Same as Fig. 8 but for the Eulerian run including *GM*.

The Eulerian circulation has the same familiar pattern in the three runs. In the Southern Ocean, it comprises a large (~42 Sv) clockwise cell driven by westerly winds at the surface. In the northern hemisphere, a second clockwise cell of about 15 Sv is associated with deep water formation in the northern Atlantic. It is completed by two shallow wind-driven, symmetric cells in the tropics, and a deep anticlockwise cell lying between 2000 and 5000 m.

The eddy-induced circulation is also broadly similar in the three runs: it is dominated by an anticlockwise cell in the southern hemisphere and also has a weaker, shallow, clockwise cell in the northern midlatitudes. These cells are of similar magnitude in *GM* and *Res*, but larger by a factor 2 or 3 in *GM_N2*. This reflects the large near-surface eddy diffusivity implied by the N^2-dependence (see Fig. 7). Note that the eddy-induced streamfunction does not increase linearly with the diffusivity since isopycnal slopes decrease with increasing diffusivity. Two interesting differences between the residual and the Eulerian runs are observed. First, the two cells are very surface intensified in *GM* and *GM_N2* since all interior flows are returned in the top layer. This results from the boundary conditions employed in the GM scheme in which the eddy streamfunction is set to zero at the ocean surface. In the TEM form, the diabatic layer introduced at the surface ensures that the return flow is spread vertically. Combined with a subsurface maxima of the equivalent eddy diffusivity κ_{gm}^{eq} (see Fig. 6), this results in a maximum streamfunction between 300 and 500 m. Secondly, the eddy-induced streamfunction in *Res* is much larger, albeit of the same pattern, than in *GM* and *GM_N2* in the tropics (middle panels). It is antisymmetric about the equator reaching a maximum at the surface close to the equator (~30 Sv).
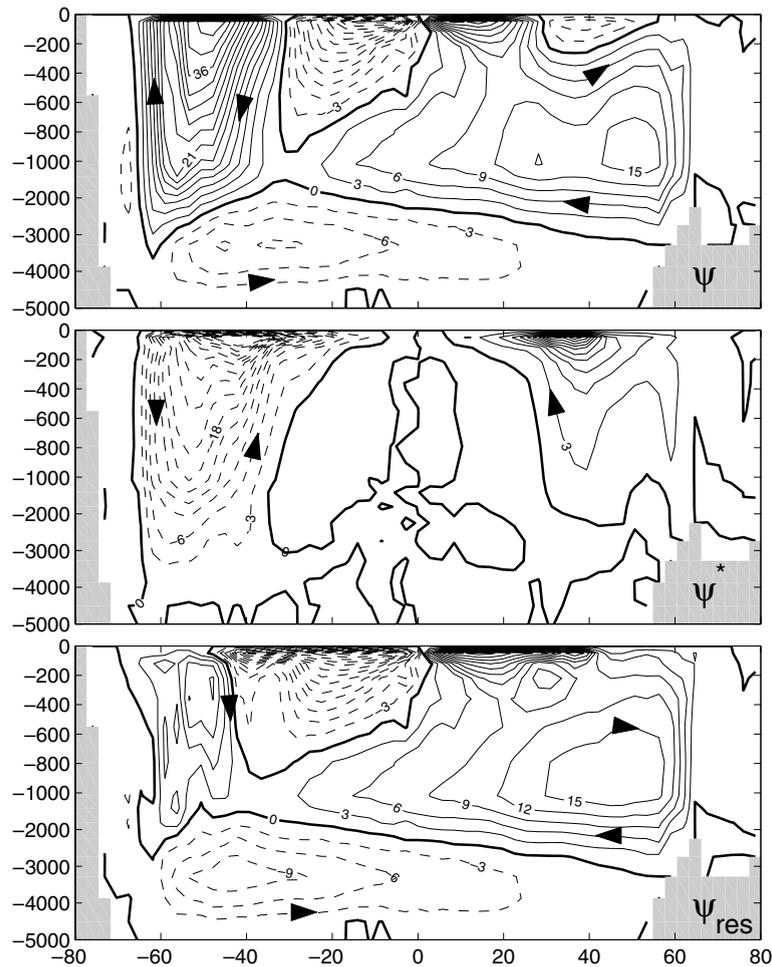
Fig. 10. Same as Fig. 8 but for the Eulerian run *GM_KN2*.

These two cells extend poleward and downward to reach a secondary maximum of about 8 Sv at a depth of 400 m at a latitude of ±10°. In the *GM* and *GM_N2* cases, the surface eddy-induced circulation near the equator is almost zero in *GM* and about 2 Sv in *GM_N2* while the maxima below never exceeds 2 Sv in both cases. These differences directly reflect the magnitude of the eddy diffusivities: the substantial eddy-driven circulation in the TEM run would require very large eddy diffusivities of up to 15,000 $m^2 s^{-1}$ in the GM scheme, as shown by the equivalent diffusivity κ_{gm}^{eq} in Fig. 6. Even the large eddy diffusivities employed in the *GM_N2* run are not sufficient to sustain a significant eddy-driven streamfunction in the tropics. Note that because of the coarse resolution of our model, diffusivities are perhaps biased toward large values. For example, McWilliams and Danabasoglu (2002) suggest the use of much smaller value (about 2000 $m^2 s^{-1}$) in a 0.5–1° resolution model.

The residual circulations (bottom panels) are very similar in strength and pattern. The most striking feature is the partial cancellation between the Eulerian and eddy-induced circulations in the Southern Ocean. This reflects, in both formulations, the steepening of isopycnals by the wind forcing and the compensating flattening and release of potential energy by baroclinic instability. The Southern ocean circulation also illustrates some fundamental differences. The vertical spreading of the eddy-induced streamfunction in *Res* results in a smaller cancellation with the Eulerian circulation near the surface than in *GM*. The residual circulation then becomes a relatively strong surface intensified clockwise cell in the TEM case and a weak (∼12 Sv) cell extending down to 1000 m in the GM case. The Deacon cell is weakly connected to the North Atlantic cell in *GM* but not in *Res*. However, note that in both cases, about 10 of the 15 Sv of North Atlantic Deep Water (partially mixed with Antarctic Bottom Water) are exported out of the Atlantic basin at 40° S.

Our current knowledge of the thermohaline circulation makes it difficult to assess which of the circulations described above is more realistic. Clearly, the three share many realistic and unrealistic features. An example of the latter is the large upwelling of Antarctica Bottom Water to the surface in the tropical Pacific which is not observed (e.g. Ganachaud and Wunsch, 2000). This is a common bias of GCMs run at coarse vertical resolution with large vertical diffusivity. The residual formulation does as poorly as the GM runs in this respect.

The large eddy-induced circulation seen in *Res* in the tropics is perhaps a satisfactory aspect since modeling studies (McWilliams and Danabasoglu, 2002) and observations (Roemmich and Gilson, 2001) suggest that it is indeed significant (a few Sverdrups or 10% of the Eulerian mean circulation). In our coarse-resolution model, this requires relatively large eddy diffusivity in the tropics of about 10,000 m^2 s^{-1}, while McWilliams and Danabasoglu (2002) suggest 2000 m^2 s^{-1} in higher resolution model. In any case, this cannot be achieved through use of a uniform eddy diffusivity since isopycnal slopes in the ACC region would be flattened out and the ACC transport would be drastically reduced (see for example FMH).

4.5. Tapering scheme

As discussed above, the improvement of the residual model *Res* relative to *GM* is almost certainly a consequence of the N^2-dependent eddy diffusivity implicit in the eddy stress parameterization (18). It is also noteworthy that the eddy-induced circulation is more realistic near the surface in the residual-mean formulation. This is illustrated in Fig. 11 which shows vertical profiles of the eddy-induced meridional streamfunction (left) and potential density (right) for *Res* and *GM*. This particular location in the Southern ocean wintertime (45–100° S, monthly mean for August) is chosen for its deep mixed layer. Although the two density profiles are rather similar, the eddy-induced circulations are very different. In *GM* it peaks at the mixed-layer base following the steepening of isopycnals and abruptly transitions to zero in the mixed layer. This unphysical behavior results from the tapering required in the GM scheme to avoid unrealistically large velocities in the presence of steep isopycnals. Other tapering schemes (e.g. Danabasoglu and McWilliams, 1995; Large et al., 1997) currently used in ocean GCMs have similar consequences. The eddy-induced circulation in the residual mean framework, however, avoids large shear and transitions smoothly to zero at the sea-surface. This is a consequence of the linear tapering of the eddy stress in the surface diabatic layer. Admittedly, this is not a particular feature of the residual formulation and similar tapering schemes of the eddy-induced streamfunction could be implemented in the GM scheme, as discussed in Ferrari and McWilliams (submitted for publication). However, this would not allow one to avoid tapering of isopycnal slopes completely because the latter can be very steep below the diabatic layer (for example when convective adjustment occurs at depth).

This points to a fundamental difference between the eddy closure proposed here in the TEM framework and the GM scheme employed in the Eulerian formulation. Numerical issues do not demand use of the tapering
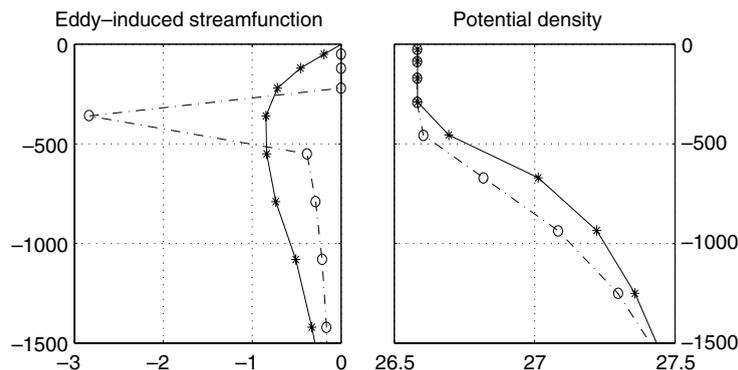

Fig. 11. Vertical profiles of the eddy-induced meridional streamfunction at about (40°, 100° E) in August (left) and the corresponding density profiles (right) for the residual run *Res* (solid) and the Eulerian run *GM* (dashed).

function μ in *Res* because the eddy-induced velocities are proportional to the shear (or the horizontal gradient of buoyancy) and are never infinite. In contrast, the tapering of isopycnal slopes in the GM scheme is primarily a device to ensure numerical stability.

5. Experiments with horizontal viscosity

5.1. Choice of horizontal viscosity

As noted in the introduction, horizontal friction is introduced in ocean models largely for pragmatic reasons. In coarse-resolution GCMs, it is mainly required to suppress grid-point noise and maintain western boundary currents (Griffies et al., 2000). Therefore, lateral mixing should be reduced to the minimum required for numerical integrity of the solution.

A yardstick to guide the choice of horizontal viscosity is to require that the width of the Munk (frictional) boundary layer be resolved by the grid (see Bryan, 1963). With an under-resolved Munk boundary layer, grid-point noise will develop. On MOM's B-grid, Griffies et al. (2000) suggest having at least two points in the Munk boundary layer to minimize spurious dissipation associated with advection. Scaling arguments suggest that for a grid-spacing Δx, the horizontal viscosity should be of order:

$$v_h = \beta(\Delta x)^3, \tag{25}$$

where β is the β-effect. For $\Delta x = 300$ km and $\beta = 2 \times 10^{-11}$ m^{-1} s^{-1}, this suggests a v_h of about 5×10^5 m^2 s^{-1} which is the value used in the reference experiments, *Res* and *GM*. As illustrated in Fig. 12, western boundary currents are spread over 5–10 grid points with this choice of horizontal viscosity, suggesting that it could be substantially reduced. Accordingly, two experiments, *ReslAh* and *GMlAh*, have been carried out with a viscosity 10 times smaller, $v_h = 5 \times 10^4$ m^2 s^{-1}. The velocity field of *GMlAh* develops a pronounced grid-point noise (not shown) which also appears in the tracer fields. Pleasingly, *ReslAh* is numerically much more robust at low viscosity. Locally, grid-point noise may appear in the vertical velocity field, but it is much better behaved than in *GMlAh*. With low viscosity, the western boundary currents are resolved by 3–5 grid points. The viscosity could not be decreased further without numerical problems occurring (not shown). This underscores that the determining factor in choosing horizontal viscosity is its control of grid-point noise. This remains true in the residual-mean model. It should be noted that because MITgcm employs a C-grid, the resulting off-set between horizontal velocity components results in the Coriolis terms being a significant source of noise which requires larger viscosity than, for example, on a B-grid.

What is clear, however, is that the residual-mean formulation requires less horizontal viscosity that the Eulerian formulation. In the residual-mean framework, the (physically meaningful) eddy stress which appears in the momentum equation, is parameterized in terms of (very) large vertical viscosity which inhibits the growth of grid-scale noise. It allows one to significantly reduce the burden placed on the (unphysical) horizontal dissipation, and thus the coefficient of horizontal viscosity. In addition to grid-point noise, the climatology of *GMlAh* drifts further from observations, as indicated by the cost functions (Table 1). In both temperature and salinity, the degradation in *GMlAh* occurs mainly in the deep ocean (below 2000 m), while the climatology benefits from the lower viscosity in the main thermocline. In the residual formulation *ReslAh*, the climatology slightly improves (mainly in the thermocline) from the use of the smaller horizontal viscosity (Table 1).

5.2. Barotropic circulation

Use of low viscosity results in some striking changes in the barotropic streamfunction. This is illustrated for the North Atlantic and Pacific basins in Fig. 12 for *Res* and *ReslAh*. Meridional profiles of the streamfunctions cutting through its maximum at about 30° N are also displayed in the bottom panel along with the transport estimated from Sverdrup balance (bottom). The *GM* streamfunction is very similar to that of *Res* and therefore not shown. Without momentum advection, the two circulations would be identical to one another since the eddy stress forcing vanishes in the vertical integral (leaving Sverdrup balance). The similarity of the two barotropic streamfunctions also indicates that the small Rossby number limit assumed in Eq. (13) is appropriate here.
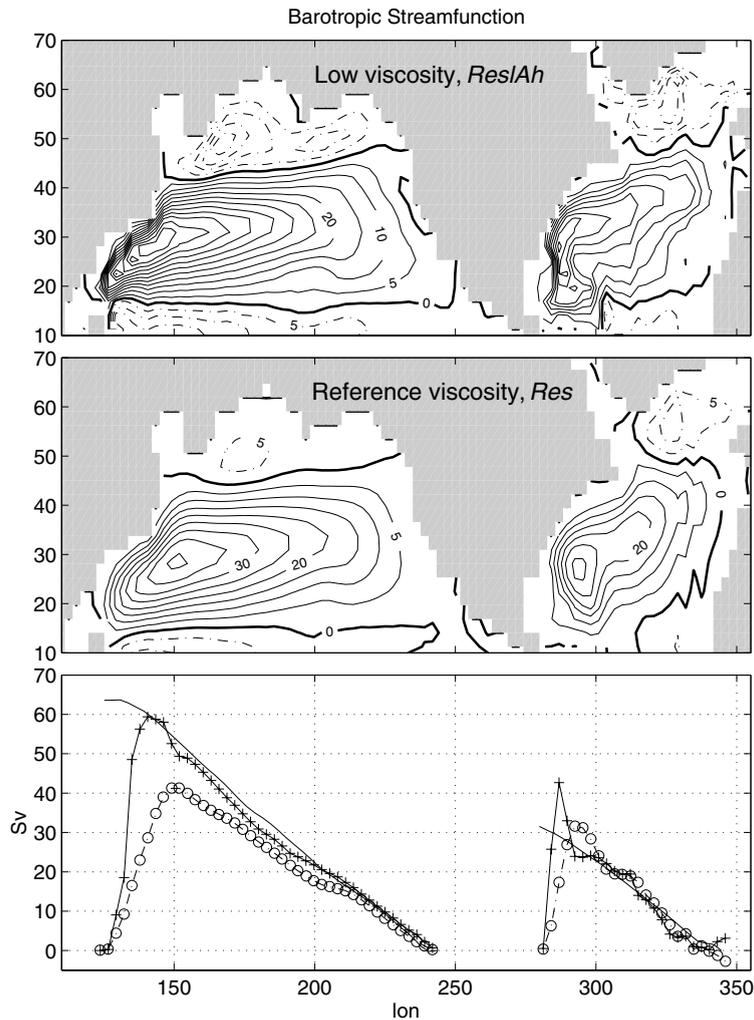
Fig. 12. Barotropic streamfunction in the North Atlantic and North Pacific basins for the low (top) and reference (middle) viscosity residual-mean model, *ReslAh* and *Res* respectively. The contour interval is 5 Sv. The solid and dashed-dotted lines are positive and negative values, respectively. The zero contour is highlighted. The bottom panel show profile at about 30° (circles and crosses for *ReslAh* and *Res*, respectively) superimposed on the barotropic streamfunction, as obtained from Sverdrup balance (solid line).

As expected, the western boundary currents are tighter when low viscosity is used, even though they remain broader than observed. Note that they are resolved by 3–5 grid points. In addition, the circulation becomes stronger with maxima of 60 and 40 Sv for the Pacific and Atlantic Ocean respectively, compared to only 40 and 30 Sv obtained when the reference viscosity is used. In the interior of the Pacific Ocean, the *ReslAh* streamfunction is much closer to Sverdrup transport than that of *Res* (or *GM*), and thus more consistent with observations (see, for example, Hautala et al., 1994). In the Atlantic ocean, the two streamfunctions are similar and close to the Sverdrup transport eastward of 300° E, but the various transports diverge west of that limit. In the low viscosity case, stronger recirculations occur near the western boundary current which carry more water northward than required to balance the quasi-Sverdrupian interior.

An appealing consequence of the reduced viscosity is the appearance of subpolar gyres in both basins. In the Pacific, the strength of the circulation jumps from 5 to 20 Sv. In the Atlantic, the subpolar gyre doubles in magnitude, but, importantly, it is no longer confined to the eastern part of the basin but instead extends westward into the Labrador sea, perhaps a more realistic feature.

Changes of the Northern Hemisphere barotropic streamfunction due to reduced horizontal viscosity are typical of all ocean basins (not shown). In particular, the ACC has a more realistic transport through Drake
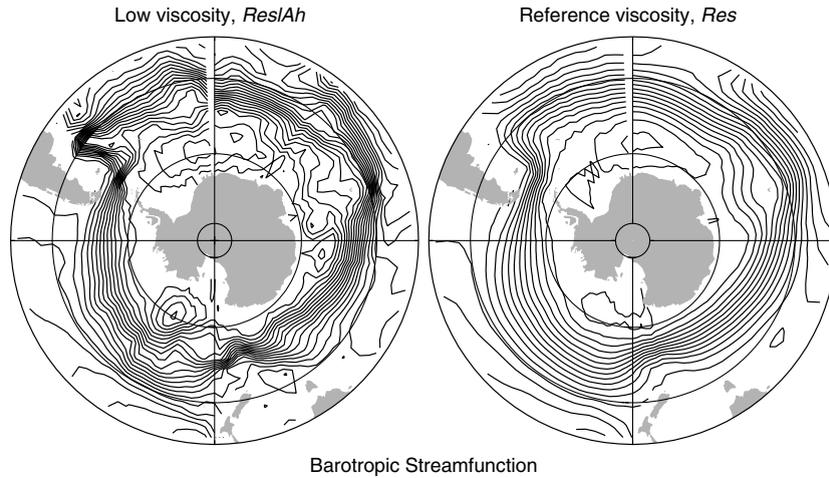
Fig. 13. Barotropic streamfunction in the Southern Ocean for the low (left) and reference (right) viscosity residual-mean model, *ReslAh* and *Res*, respectively. The contour interval is 10 Sv.

Passage, increasing from about 111 Sv to 124 Sv (see Table 1 and Fig. 13). Compared to the smooth and wide flow obtained using the reference viscosity, the ACC in the case of low viscosity is tighter and its path is more clearly influenced by topographic features.

6. Role of diabatic eddy fluxes

Finally, we carry out an experiment in which the residual flux is incorporated. We only discuss the results in the case of low viscosity (*ReslAhF*) because the global effects of the residual flux are almost null if the reference viscosity is used. At low viscosity, they are still relatively small (compare *ReslAhF* and *ReslAh* in Table 1) but more apparent, perhaps, because of the presence of stronger meridional gradients.

The climatology of the model is degraded, both in temperature and salinity, when the residual flux is included (Table 1). This is primarily due to the increase of the cold and fresh bias of Antarctic Bottom Water.
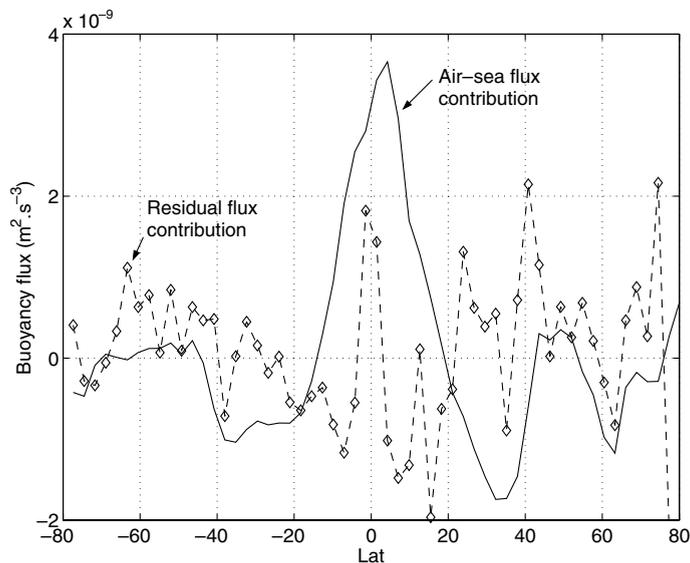

Fig. 14. Zonally averaged residual flux forcing ($-\nabla \cdot \mathbf{F}_{res}$) converted to a surface buoyancy flux (dashed line) for comparison with the air-sea buoyancy flux (solid). So that the same scale could be used for both curves, the air-sea buoyancy flux is divided by 10.

Surface waters in the tropics and midlatitudes are denser while high-latitude bottom waters are lighter (not shown). This is consistent with the down-gradient closure of the residual flux. Here, however, the result is to further increase the bias of the model.

The zonal mean divergence of $\mathbf{F}_{res}$ integrated over the diabatic layer and converted to a surface flux, is displayed in Fig. 14, along with the surface buoyancy flux. The latter is downscaled by a factor 10. As expected, the residual flux results, on the large scale, in a loss of buoyancy in the tropics and a gain at high latitudes. The positive peak at the equator corresponds to the warming of the cold tongue. In the mean, the residual flux forcing is small compared to the surface forcing, typically contributing some 10%. A notable exception is the ACC region where the two terms are of comparable magnitude (see the discussion in Marshall and Radko, 2003). On a smaller scale, the residual flux is thought to be relatively important in the Kuroshio, the Gulf stream, the Agulhas current and at the tip of South America (not shown).

The residual flux is probably underestimated in our calculations, due to the coarse horizontal resolution of the model and the associated weak buoyancy gradient. Poor knowledge of the diabatic layer depth and the choice of diffusivity κ_s – which varies strongly in space (see Marshall et al., in press) – may play a role.

7. Conclusions

The residual-mean framework was used to revisit the parameterization of mesoscale eddies in coarse-resolution ocean climate models. In the residual-mean formulation, the resolved circulation is the residual circulation, the sum of Eulerian and eddy-induced circulations. The residual-mean momentum equation has an additional forcing term, the vertical divergence of an eddy stress. In the adiabatic limit, appropriate to the ocean interior, the residual flow advects all tracers. However, near horizontal boundaries where mesoscale eddies develop a diabatic component, there is also transport by a residual flux which is not accounted for by the eddy-induced velocity.

The divergence of the eddy stress is represented here as a vertical viscosity which is only a function of latitude, varying from zero at the equator to a few $m^2\,s^{-1}$. The eddy stress is tapered linearly within the diabatic layer so that the eddy-induced velocity is uniform in the vertical and does not restratify the top layers. Using the quasi-adiabaticity of mesoscale eddies in the ocean interior, the residual flux is only considered near the surface in the diabatic layer where it is parameterized as a down-gradient flux.

These parameterizations are implemented and tested with the MITgcm at coarse resolution. Solutions are compared with that of the same model run in the Eulerian framework in which eddy effects are represented by the GM scheme. Equilibrated simulations show that the residual-mean model has (1) a significantly improved climatology (temperature and salinity) compared to the Eulerian/GM one using a uniform eddy diffusivity and (2) a similar climatology to that obtained from a Eulerian/GM one using a N^2-dependent eddy diffusivity. This suggests that the improvement of the residual-mean model mainly results from the implicit N^2-dependent eddy diffusivity associated with the eddy stress parameterization although the introduction of the diabatic layer and the improved treatment of the boundary conditions of the eddy-induced circulation may also play a role. It is also noteworthy that, in contrast to the Eulerian/GM formulation, our parameterization does not require ad hoc tapering scheme to avoid the divergence of the model. In addition, these experiments underscore a point already made by FMH that the implementation of surface-intensified eddy diffusivity clearly improve coarse-resolution ocean models.

A very interesting property of the residual-mean formulation is that it requires less (spurious) horizontal viscosity than the Eulerian one. This stems from the presence of an eddy stress in the residual-mean momentum equation, which partially inhibits growth of grid-point noise, thus reducing the need for horizontal friction. An order of magnitude decrease of horizontal viscosity can be achieved by the use of a residual-mean framework.

The residual flux has a relatively modest effect on the large scale except in the Southern Ocean where it is comparable to the air-sea buoyancy flux. However, it may be of importance locally near western boundary currents, the ACC and in the tropics. A better assessment of the role and importance of the residual flux requires higher resolution calculations and a better understanding of the diabatic layer. The latter is probably the most serious caveats of the parameterization. The representation of the diabatic layer may be crucial as it influences both the eddy stress (and hence the eddy-induced circulation), and the residual flux. Theoretical and

observational guidance about boundary diabatic layers are strongly needed. Analysis of high-resolution eddy-resolving models may also provide useful hindsight. Note that this issue is also relevant to models based on an Eulerian framework and the GM scheme (Ferrari and McWilliams, submitted for publication).

In conclusion, then, this study is a first attempt to formulate and study a coarse-resolution climate ocean model using the residual-mean framework. It shows that such a formulation can substantially improve such models and could provide a way forward to parameterized eddy processes. However, we have not exploited the full potential of the residual-mean framework here. We have not attempted to relate the eddy stress forcing to an eddy potential vorticity flux. Homogenization of potential vorticity on subsurface isopycnals is a feature of observations (Keffer, 1985) and offers a great incentive to phrase the eddy-mean flow interaction in terms of potential vorticity mixing. Moreover, as underscored by Greatbatch (1998), the residual-mean approach also offers a framework to include Reynolds stresses in one parameterization.

Acknowledgments

Appendix A. Implementation of the eddy stress

Combining Eqs. (7) and (16), the eddy stress is given by

$$\frac{\tau^e}{\rho_0} = \begin{cases} v_e \partial_z \mathbf{v}_{res}, & z \leqslant -h_s, \\ v_e \mu(z) \partial_z \mathbf{v}_{res}|_{-h_s}, & -h_s \leqslant z \leqslant 0, \end{cases} \tag{26}$$

where μ is the tapering function and h_s, the depth of the surface diabatic layer. In this study, we use $h_s = 120$ m and $\mu = -z/h_s$.

By rearranging the eddy stress in the diabatic layer thus

$$\frac{\tau^e}{\rho_0} = v_e \mu(z) \frac{\partial_z \mathbf{v}_{res}|_{-h_s}}{\partial_z \mathbf{v}_{res}} \partial_z \mathbf{v}_{res}, \tag{27}$$

the eddy stress forcing in the residual-mean momentum equation (13) is then equivalent to a vertical viscosity $\tilde{v}_e$:

$$\tilde{v}_e = \begin{cases} v_e, & z \leqslant -h_s, \\ v_e \mu(z) \frac{\partial_z \mathbf{v}_{res}|_{-h_s}}{\partial_z \mathbf{v}_{res}}, & -h_s \leqslant z \leqslant 0. \end{cases} \tag{28}$$

This permits a simple implementation of the eddy stress and its tapering as an "effective" viscosity $\tilde{v}_e$ which is treated implicitly to ensure numerical stability. In the diabatic layer, $\tilde{v}_e$ can occasionally be very large if $\partial_z \mathbf{v}_{res}$ tends to zero or very small or negative if the shear changes sign at the diabatic layer depth. To avoid such extreme values, $\tilde{v}_e$ is constrained to remain between 10^{-2} m^2 s^{-1} and 50 m^2 s^{-1}. The upper limit is about 10 times the maximum of v_e. The lower limit is chosen so that the eddy stress is at least 10 times larger than the background vertical viscosity (10^{-3} m^2 s^{-1}). The solution is rather insensitive to these choices of range.

References

Adcroft, A., Hill, C., Marshall, J., 1997. Representation of topography by shaved cells in a height coordinate ocean model. Mon. Wea. Rev. 125, 2293–2315.

Andrews, D.G., McIntyre, M.E., 1976. Planetary waves in horizontal and vertical shear: the generalized Eliassen–Palm relation and the mean zonal acceleration. J. Atmos. Sci. 33, 2031–2048.

Andrews, D.G., Holton, J.R., Leovy, C.B., 1987. Middle Atmosphere Dynamics. Academic Press, 489 pp.

Bryan, K., 1963. A numerical investigation of a nonlinear model of a wind-driven ocean. J. Atmos. Sci. 20, 594–606.

Danabasoglu, G., McWilliams, J., 1995. Sensitivity of the global ocean circulation to parameterizations of mesoscale tracer transports. J. Climate 8, 2967–2987.

Ferrari, R., McWilliams, J.C., submitted for publication. Parametrization of eddy fluxes near the oceanic boundaries. J. Phys. Oceanogr.

Ferreira, D., Marshall, J., Heimbach, P., 2005. Estimating Eddy stresses by fitting dynamics to observations using a residual-mean ocean circulation model and its adjoint. J. Phys. Oceanogr. 35, 1891–1910.

Ganachaud, A., Wunsch, C., 2000. The oceanic meridional overturning circulation, mixing, bottom water formation, and heat transport. Nature 408, 453–457.

Gent, P.R., McWilliams, J.C., 1990. Isopycnic mixing in ocean circulation models. J. Phys. Oceanogr. 20, 150–155.

Gent, P.R., Willebrand, J., McDougall, T.J., McWilliams, J.C., 1995. Parameterizing eddy-induced tracer transports in ocean circulation models. J. Phys. Oceanogr. 25, 463–474.

Gerdes, R., Koberle, C., Willebrand, J., 1991. The influence of numerical advection schemes on the results of ocean general circulation models. Climate Dyn. 5, 211–226.

Gill, A.E., Green, J.S.A., Simmons, A.J., 1974. Energy partition in the large-scale ocean circulation and the production of mid-ocean eddies. Deep-Sea Res. 21, 499–528.

Greatbatch, R.J., Lamb, K.G., 1990. On parameterizing vertical mixing of momentum in non-eddy-resolving ocean models. J. Phys. Oceanogr. 20, 1634–1637.

Greatbatch, R.J., 1998. Exploring the relationship between eddy-induced transport velocity, vertical momentum transfer, and the isopycnal flux of potential vorticity. J. Phys. Oceanogr. 28, 422–432.

Green, J.S.A., 1970. Transfer properties of the large-scale eddies and the general circulation of the atmosphere. Quart. J. Roy. Meteor. Soc. 96, 157–185.

Griffies, S.M., Böning, C., Bryan, F.O., Chassignet, E.P., Gerdes, R., Hasumi, H., Hirst, A., Treguier, A.-M., Webb, D., 2000. Developments in ocean climate modelling. Ocean Modell. 2, 123–192.

Hautala, S.L., Roemmich, D.H., Schmitz Jr., W.J., 1994. Is the North Pacific in Sverdrup balance along 24° N? J. Geophys. Res. 99, 16041–16052.

Jiang, S., Stone, P.H., Malanotte-Rizzoli, P., 1999. An assessment of the geophysical fluid dynamics laboratory ocean model with coarse resolution: annual-mean climatology. J. Geophys. Res. 104, 25623–25645.

Keffer, T., 1985. The ventilation of the world's oceans: maps of the potential vorticity field. J. Phys. Oceanogr. 15, 509–523.

Kuo, A., Plumb, R.A., Marshall, J., 2005. Transformed Eulerian mean theory. Part II. Potential vorticity homogenization, and the equilibrium of a wind- and buoyancy-driven zonal flow. J. Phys. Oceanogr. 35, 175–187.

Large, W.G., Danabasoglu, G., Doney, S.C., McWilliams, J.C., 1997. Sensitivity to surface forcing and boundary layer mixing in a global ocean model: annual mean climatology. J. Phys. Oceanogr. 27, 2418–2447.

Levitus, S., Boyer, T.P., 1994. Temperatures. World Ocean Atlas 1994, vol. 4. NOAA Atlas NESDIS 4, 117 pp.

Levitus, S., Burgett, R., Boyer, T.P., 1994. Salinity. World Ocean Atlas 1994, vol. 3. NOAA Atlas NESDIS 3, 99 pp.

Marshall, J.C., 1981. On the parameterization of geostrophic eddies in the ocean. J. Phys. Oceanogr. 11, 1257–1271.

Marshall, J., Adcroft, A., Hill, C., Perelman, L., Heisey, C., 1997a. A finite-volume, incompressible Navier Stokes model for studies of the ocean on parallel computers. J. Geophys. Res. 102 (C3), 5753–5766.

Marshall, J., Hill, C., Perelman, L., Adcroft, A., 1997b. Hydrostatic, quasi-hydrostatic, and nonhydrostatic ocean modeling. J. Geophys. Res. 102 (C3), 5733–5752.

Marshall, J., Radko, T., 2003. Residual-mean solutions for the Antarctic circumpolar current and its associated overturning circulation. J. Phys. Oceanogr. 33, 2341–2354.

Marshall, J., Shuckburgh, E., Jones, H., Hill, C., in press. Estimates and implications of surface eddy diffusivity in the southern ocean derived from tracer transport. J. Phys. Oceanogr.

McWilliams, J., Danabasoglu, G., 2002. Eulerian and Eddy-induced meridional overturning circulation in the Tropics. J. Phys. Oceanogr. 32, 2054–2071.

Plumb, R.A., 1979. Eddy fluxes of conserved quantities by small amplitude waves. J. Atmos. Sci. 33, 1699–1704.

Radko, T., Marshall, J., 2003. Equilibration of a warmed pumped lens on a β-plane. J. Phys. Oceanogr. 33, 885–899.

Redi, M.H., 1982. Oceanic isopycnal mixing by coordinate rotation. J. Phys. Oceanogr. 12, 1154–1158.

Rhines, P.B., 1979. Geostrophic turbulence. Ann. Rev. Fluid Mech. 11, 404–441.

Rhines, P.B., Young, W.R., 1982. Homogenization of potential vorticity in planetary gyres. J. Fluid Mech. 122, 347–386.

Roemmich, D., Gilson, J., 2001. Eddy transport of heat and thermocline waters in the North Pacific: a key to interannual/decadal climate variability. J. Phys. Oceanogr. 31, 675–688.

Stammer, D. et al., 2002. Global ocean circulation during 1992–1997, estimated from ocean observations and a general circulation model. J. Geophys. Res. 107, 3118. doi:10.1029/2001JC000888.

Treguier, A.M., Held, I.M., Larichev, V.D., 1997. On the parameterization of the quasigeostrophic eddies in primitive equation ocean models. J. Phys. Oceanogr. 27, 567–580.

Trenberth, K.E., Large, W.G., Olson, J.G., 1990. The mean annual cycle in global ocean wind stress. J. Phys. Oceanogr. 20, 1742–1760.

Wardle, R., Marshall, J., 2000. Representation of eddies in primitive equation models by a PV flux. J. Phys. Oceanogr. 30, 2481–2503.